

Mode mixing in asymmetric double trench photonic crystal waveguides

Yu. A. Vlasov,^{1,*} N. Moll,² and S. J. McNab¹

¹*IBM T. J. Watson Research Center, Yorktown Heights, NY 10598, USA*

²*IBM Research, Zurich Research Laboratory, Säumerstrasse 4, 8803 Rüschlikon, Switzerland*

(Dated: October 15, 2018)

We investigate both experimentally and theoretically the waveguiding properties of a novel double trench waveguide where a conventional single-mode strip waveguide is embedded in a two dimensional photonic crystal (PhC) slab formed in silicon on insulator (SOI) wafers. We demonstrate that the bandwidth for relatively low-loss (50dB/cm) waveguiding is significantly expanded to 250nm covering almost all the photonic band gap owing to nearly linear dispersion of the TE-like waveguiding mode. The flat transmission spectrum however is interrupted by numerous narrow stop bands. We found that these stop bands can be attributed to anti-crossing between TE-like (positive parity) and TM-like (negative parity) modes. This effect is a direct result of the strong asymmetry of the waveguides that have an upper cladding of air and lower cladding of oxide. To our knowledge this is the first demonstration of the effects of cladding asymmetry on the transmission characteristics of the PhC slab waveguides.

I. INTRODUCTION

Two-dimensional slab-type silicon photonic crystals (PhC) are seen as a possible platform for dense integration of photonic integrated circuits (IC) on a chip-scale level^{1,2,3,4,5,6,7,8,9}. Single-mode PhC waveguides are typically defined by introducing a line defect in an otherwise perfect periodic lattice, for example omitting one row of holes creates the so-called W1 waveguide^{1,2,3,4,5,9}. It has been shown, however, that the resulting bandwidth of the guided mode below the light line which is potentially lossless is typically very small⁴, sometimes of the order of only a few tens of nanometers⁵. At the same time group velocity dispersion is large owing to lattice-induced distributed feedback along the propagation direction⁴. Recently another waveguide design has attracted much attention, where the conventional single-mode strip waveguide is embedded into a PhC slab⁶ (also known as the double-trench waveguide). It combines the best features of PhC slabs, such as strong localization of the waveguiding mode with the potential to suppress radiation losses at bends, with a broad bandwidth and linear dispersion characteristic of strip waveguides. Here we report quantitative transmission measurements of integrated optical circuits containing this broad bandwidth double-trench PhC waveguide fabricated on 200-mm SOI wafers.

II. DESIGN OF THE PHOTONIC IC WITH THE DOUBLE-TRENCH PHC WAVEGUIDE

A. Design of the Double-trench PhC Waveguide

The novel design of the PhC waveguide formed by replacing the row of rods in a slab with a strip waveguide was analyzed in Ref. 1. It has been shown that addition of a PhC cladding to the strip waveguide does little to

disturb its almost linear group velocity dispersion. At the same time the mode is guided by the photonic band gap and correspondingly, radiation losses at sharp bends might be significantly suppressed. This idea has been extended further^{6,7} to the case of a triangular lattice of holes in high-refractive index slab which is believed to be a more fabrication-friendly design. It has been proposed to replace the line defect in a PhC slab with low-index oxide⁷ or high-index strip waveguide⁶, thus producing single-mode gap guiding with bandwidth spanning over 60% of the photonic band gap width. Consideration of the truncation of the PhC lattice has been shown to be important to eliminate the influence of surface states on the waveguiding mode^{6,8}.

For our study we adopted the design rules proposed in Ref. 6, since it does not require additional lithographic and oxide deposition steps as in Ref. 7, and at the same time utilizes the lattice of holes which is more fabrication tolerant than silicon pillars lattice of Ref. 1. The PhC lattice parameters were chosen to position the photonic band gap for TE-like (even) modes around 1500 nm wavelength. The hole diameter D was set to 306 nm with a lattice constant a of 437 nm. For a silicon slab thickness of $0.5a$ (220 nm) and a D/a ratio of 0.7, an even-symmetry photonic band gap has a bandwidth of about 30% of its central frequency, spanning from 1200 to 1600 nm, thus covering all the important telecommunications wavelengths. The core of the waveguide is formed by omitting one row of holes in the PhC lattice in the Γ - M direction and etching two parallel trenches to define the strip waveguide in the center. The resulting double-trench PhC waveguide is shown schematically in the inset of Fig. 1. The width of the strip waveguide W embedded in the PhC slab was chosen to be $0.6a$ (263 nm) designed to optimally phase-match the photonic band gap of the slab. The width of the trench W_a separating the strip from the PhC cladding was chosen to be $0.8a$ (350 nm).

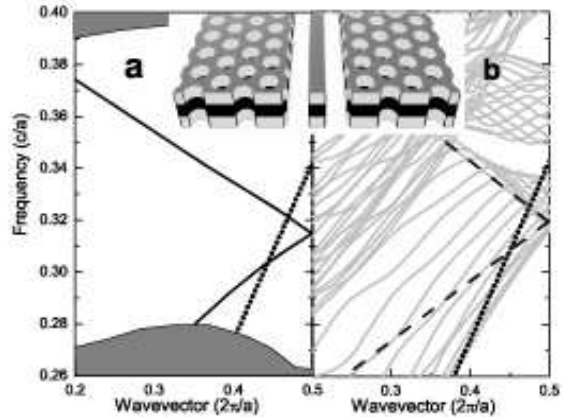


FIG. 1: Photonic band diagram of symmetric double-trench waveguide for (a) TE-like and (b) TM-like bands. The dotted lines represent the light line of the oxide cladding. Inset: Scheme of the double-trench PhC waveguide. The dashed line in (b) shows the fundamental TM-like mode confined mainly in the strip waveguide. The silicon slab is surrounded by oxide layers on top and bottom. The width of the strip waveguide is $W = 0.6$ and the width of the trench separating it from the PhC is $W_a = 0.8$. Artifact bands created because of artificial periodic boundaries introduced by the super cell have been omitted.

These parameters guarantee the truncation of the PhC lattice which is required to push the unwanted surface states out of the photonic bandgap^{6,8}.

The photonic band structure of the resulting waveguide calculated with the MIT Photonic Bands code¹⁰ is presented in Fig. 1. The following parameters were used: $W = 0.6a$, $W_a = 0.8a$, slab thickness of $0.5a$, $D = 0.7a$, and dielectric permittivity of the slab and oxide was taken as 12.13 and 2.1 respectively. To obtain reliable results 16 rows of holes perpendicular to the waveguide were included in the computational cell and 16 plane waves per lattice constant were used to compute the band structure. Since the structure is assumed to be symmetric with respect to the slab plane (oxide layers on the top and on the bottom of the slab) the solutions are separated into TE-like (even) and TM-like (odd) modes presented in Fig. 1(a) and Fig. 1(b) respectively. The TE-like mode shown in Fig. 1(a) is characterized by a very broad bandwidth defined by a light line cutoff at $0.29c/a$ on the lower frequency side and the upper edge of the photonic gap at $0.39c/a$. The dispersion of the TE-like mode resembles the linear dispersion of the conventional strip waveguide of corresponding cross-section. The major difference is appearance of the narrow stop band at the Brillouin zone (BZ) boundary at $0.32c/a$, where the TE-like mode folds. This stop band originates from periodic perturbations along the waveguide length, which are due to the PhC cladding.

The band structure for the TM-like modes is more complicated due to numerous slab modes folded at the BZ boundary. Although the photonic gap is absent, the light can still be guided mostly in the core of the waveguide due to index guiding as for a conventional strip waveguide. The corresponding fundamental mode is highlighted in Fig. 1(b) by a thick dashed line.

B. Design of the Optical Integrated Circuit

One major obstacle in experimental studies of transmission characteristics of PhC waveguides is the large coupling loss, a result of poor geometrical overlap and strong impedance mismatch between the optical modes in the launching fiber and the SOI photonic waveguides. Back-reflections at multiple poorly matched interfaces in the optical circuit result in strong Fabry-Perot oscillations in the transmission spectra. As a result intrinsic spectral features arising from the underlying photonic band structure are hidden in this Fabry-Perot noise, severely complicating the interpretation of experimental results. Recently we proposed and tested a solution to this problem which is based on two-stage coupling scheme⁵. First the light is coupled from the tapered and microlensed fiber to a single-mode strip waveguide via a spot-size converter based on an inverted taper design. Once the light is guided in the strip waveguide the coupling into the PhC waveguide is performed via simple butt-coupling. This scheme proved to be efficient for W1 membrane-type PhC waveguides with back-reflection losses on all interfaces not exceeding a few dB⁵. For the double-trench PhC waveguide design considered here coupling at the interface PhC/strip waveguide is already close to optimal since optical mode in the strip waveguide of the width W (263nm) is nearly phase-matched to the gap-guided mode in the PhC⁶. An inverted taper fiber coupler is not very efficient, however, for coupling into waveguide of such a small width. Hence we utilized the spot-size converter with the same parameters as in Ref. 5 to couple the light first from the fiber to the strip waveguide of 465 nm width. This wide strip is then adiabatically tapered down to a 260-nm-wide access waveguide which is butt-coupled to the double-trench PhC waveguide.

A loss figure for the double-trench PhC waveguides was obtained from measurements of devices of fixed length (4.6 mm) but with varying lengths of the double-trench PhC waveguides ranging from 100 μm to 2 mm (i.e. 228 to 4572 lattice periods). In order to compare the transmission characteristics of the double-trench PhC waveguide with that of conventional strip waveguides the reference optical circuit without a PhC waveguide was included in each set. The reference consisted of a strip waveguide of 260 nm width and 700 μm in length in the central section, which was adiabatically tapered to 465 nm wide access strip waveguides on both sides with input and output spot-size converters.

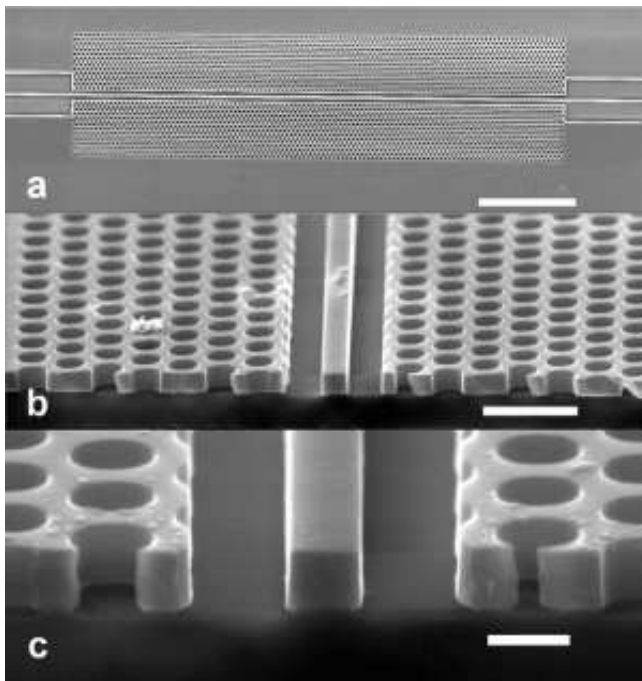


FIG. 2: SEM images of the double-trench PhC waveguide at different magnifications. The white bar is 20, 1 and 0.3 μm for images (a), (b) and (c), respectively.

III. FABRICATION AND OPTICAL TESTING

A. Fabrication

Devices were patterned on 200 mm silicon on insulator (SOI) Unibond wafers manufactured by SOITEC. The 220-nm-thick Si was lightly *p*-doped with a resistivity of $\sim 10 \Omega\text{cm}$ and a 2 μm buried oxide layer, which optically isolates devices from the substrate. A 50-nm-thick oxide deposited on the substrate acted as a hard mask for subsequent etching.

The double-trench PhC waveguides, strip waveguides and silicon tapers of the spot-size converters were defined in one step by electron beam lithography. The combined length of the whole circuit with fiber couplers on both ends was 4.6 mm. The resist pattern was transferred to the oxide hard mask using $\text{CF}_4/\text{CHF}_3/\text{Ar}$ chemistry. The resist was then removed and the patterned oxide mask transferred to the Si layer with a HBr-based etch. Sidewall angles close to 90° were obtained and sidewall roughness is estimated to be below 5 nm (see Fig. 2(c)). A final lithography step defined the epoxy polymer for the fiber coupler. Samples consisting of sets of 5 double-trench PhC waveguides of different lengths and a reference optical circuit each were then cleaved on both sides to enable edge-coupling. Further details of the fabrication procedure are reported elsewhere⁵.

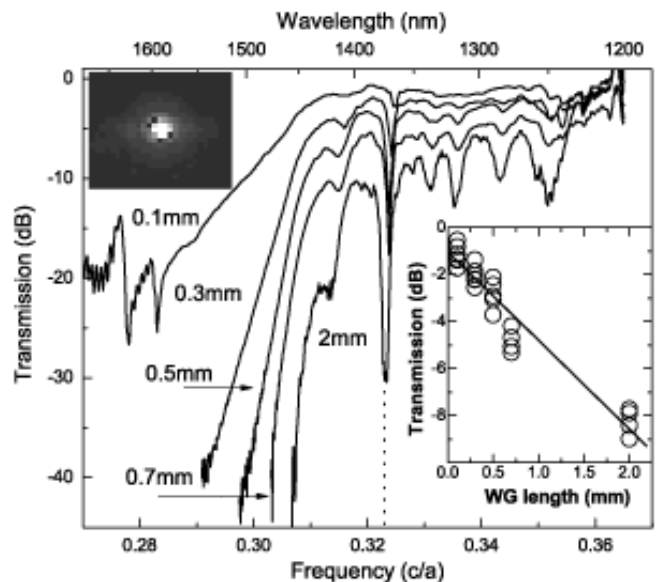


FIG. 3: Set of transmission spectra of double-trench PhC waveguides of different lengths for TE polarization. Spectra are normalized on transmission through a reference circuit with a 260 nm wide strip waveguide. Top inset: IR camera image of the TE-mode profile in 500- μm -long PhC waveguide. White bar is 20 μm . Bottom inset: attenuation measured at 1300 nm wavelength as a function of the PhC waveguide length for 20 different samples.

B. Experimental Setup for Optical Testing

The light from a broadband ASE source was first coupled to a polarization maintaining (PM) fiber, directed to a polarization controller and then coupled to the input port of the Si device under test (DUT) via a tapered and lensed PM fiber tip producing a spot with a beam waist of 2.1 μm . After passing through the DUT the light from the output port is collected by a tapered SM fiber with a beam waist of 1.85 μm and the transmission spectrum captured by an optical spectrum analyzer. The near-field profiles of the propagating mode shown in the inset of Figs. 3 and 4 were acquired with an IR camera through a 40X objective at the exit of a cleaved double-trench PhC (500 μm long). The resulting image represents a wavelength averaged field distribution in the waveguide as the source is a broadband LED. Further details of the optical set-up are described elsewhere⁵.

IV. EXPERIMENTAL RESULTS

A. TE Transmission of a Double-trench PhC Waveguide

The image in the top inset of Fig. 3 demonstrates that the propagation is predominantly single-moded and almost all the light for TE polarization is confined in the

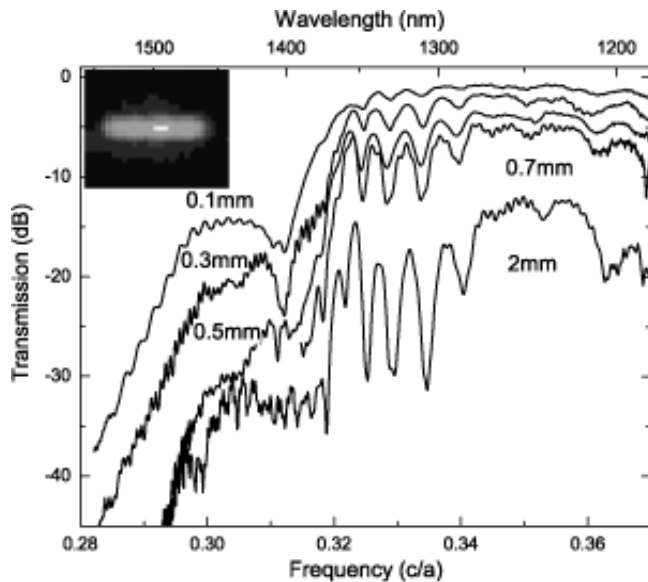


FIG. 4: Transmission spectra for double-trench PhC waveguides of different lengths for TM-polarized light. Spectra are normalized on transmission through a reference circuit with a 260-nm-wide strip waveguide. Inset: IR camera image of the TM-mode profile in 500- μm -long PhC waveguide. The white bar is 20 μm wide.

very center of the PhC waveguide with minimal intensity in the photonic crystal itself.

The set of transmission spectra measured for the TE polarization (electric field in the slab plane) for the double-trench PhC waveguides of different lengths is presented in Fig. 3. The spectrum for the 100- μm -long device is characterized by a nearly flat transmission curve. The bandwidth of high transmission spans from 1200 nm to the apparent cutoff at 1445 nm and is interrupted only by a small dip around 1370 nm. This broad bandwidth transmission is exactly what is expected from the photonic band structure of Fig. 1(a). Indeed comparing the band diagram and experimental spectra it is clearly seen that the cutoff is well described by the crossing of the corresponding mode with the oxide light-line.

The attenuation dip at 1370 nm is only barely visible for the 100 μm length PhC spectrum, but dominates for longer waveguides. This dip can be explained by the narrow stop band due to the zone-folding of the TE-like mode at $k = 0.5$. As expected, attenuation at the center of the dip increases exponentially with the length with losses of the order of 100 dB/cm. The width of this stop band is a direct measure of the interaction of the embedded strip waveguide and surrounding PhC cladding and can be estimated from scalar coupled-wave theory¹⁰. Attenuation of 100 dB/cm gives a coupling constant of $0.002a^{-1}$, which results in a stop band width of $2 \times 10^{-4}(c/a)$. This number is close to $5 \times 10^{-4}(c/a)$ obtained from full-vectorial 3D plane wave calculations of Fig. 1(a). Experimentally the width of the stop band

broadens with increasing length of the double-trench PhC waveguide consistent with the increased interaction length. At longer wavelengths, around 1600 nm, several resonances can be seen in the spectrum for the 100- μm -long waveguide, which can be readily attributed to the slab modes at the photonic band edge around $0.28c/a$ (see Fig. 1(a)).

Besides features common to the spectra for all lengths of the double-trench PhC waveguides, numerous strongly attenuated dips appear in transmission spectra of long devices. These dips divide the spectrum into separate high transmission bands. Increasing the waveguide length progressively lowers the average transmission indicating increased scattering losses. These losses can be measured by plotting transmission at the center of one of the high transmission bands, at a wavelength of 1300 nm for example as shown in the inset of Fig. 3. By fitting the length dependence the slope of 38 ± 2 dB/cm is obtained. However, since the length of the 465-nm-wide access strip waveguide becomes correspondingly smaller as the PhC waveguide length increases, this number should be corrected by subtracting losses in strip waveguide as explained in Ref. 5. Scattering losses of the TE-like mode in 465 nm waveguide at 1300 nm wavelength were measured previously to be 12 ± 1 dB/cm. The corrected loss figure for the TE-like mode in the double-trench PhC waveguide is therefore 50 dB/cm, which is among the lowest reported for PhC waveguides.

The numerous dips at wavelengths of 1250, 1283, 1318, 1336, and 1414 nm, observed in the spectra of Fig. 3 cannot be assigned to the Fabry–Perot oscillations, since their spectral positions do not change with the length of the PhC waveguide. Rather these resemble the appearance of narrow stop bands. Indeed, after subtraction of scattering losses at the maximum of a nearby high transmission band, it can be shown that the attenuation at the center of a dip at 1318 nm, for example, increases exponentially with the length with additional losses of 39 ± 1 dB/cm. Simple estimate based on a coupled-wave theory¹¹ gives the width of a corresponding stop band of only $8 \times 10^{-5}(c/a)$. Other dips exhibit nearly the same attenuation and, correspondingly, could be assigned to stop bands of analogous width. Explanation of these findings and interpretation of the stop bands requires detailed analysis of the photonic band structure, which will be presented in Sect. V.

B. TM Transmission of a Double-trench PhC Waveguide

The near-field image of the TM-like mode shown in the inset of Fig. 4 indicates that the waveguide is multimoded with some modes propagating in the photonic crystal slab. However most of the light is still confined in the central strip which is characteristic of predominantly single-mode propagation by the TM fundamental mode (black dashed line in Fig. 6).

TM transmission spectra for double-trench PhC waveguides of different lengths are shown in Fig. 4. The TM spectrum for the 100- μm -long waveguide can be explained by referring to the photonic band diagram of Fig. 1(b). The sharp cutoff visible at 1365 nm results from the fundamental TM mode crossing the oxide lightline. At longer wavelengths waveguiding is provided mainly by slab modes in the PhC, however they do not contribute significantly to our transmission measurements as coupling to the strip access waveguides is inefficient. These modes exhibit high reflectivity from the end facets of the photonic crystal giving rise to visible Fabry–Perot oscillations. The second cutoff seen at 1465 nm is owing to the cutoff of the 465-nm-wide strip access waveguide.

Increasing the waveguide length results in more complicated spectra with numerous strongly attenuated dips appearing. As for the TE spectra, these dips can be assigned to narrow stop bands with nearly analogous width of the order of $5\text{--}7 \times 10^{-5}(c/a)$ estimated from the attenuation constant. The overall propagation losses of the TM mode are much higher than TE as seen from pronounced vertical shift of the spectra with increasing length. They can be estimated by analogous measurements at 1300 nm as 72 dB/cm. Since scattering losses in the access strip waveguide of 465 nm width were measured for TM polarization to be around 4 dB/cm, the corrected loss figure of the TM mode is 76 ± 5 dB/cm.

V. INTERACTION OF TE- AND TM-LIKE MODES IN ASYMMETRIC SOI PHC SLABS

The preceding analysis of the results presented in Figs. 3 and 4 imply that most of the spectral features (cut-offs and the stop band at BZ edge) in the transmission spectra can be explained by the physical model of non-interacting TE-like and TM-like bands of Fig. 1. The same conclusion can be drawn from the analysis of near-field profiles for TE-like and TM-like modes seen in the insets of Figs. 3 and 4. It is seen that the TE-mode is predominantly confined in the center of the waveguide as is expected for the fundamental TE-like mode in the embedded strip waveguide. However the simple physical model of Fig. 1 fails to predict the appearance of numerous narrow stop bands visible in transmission spectra of long PhC waveguides. The observed phenomena can be explained by taking into account the inherent asymmetry of the SOI PhC structure. Indeed the experimentally realized structure of Fig. 2 differs from the design of Fig. 1 in one critical aspect—the SOI structure is not symmetric with respect to the slab plane. The silicon slab sits on 2 μm of oxide while above it is surrounded by air. The mode confined in the slab, therefore, sees different refractive indices below and above the slab. For symmetric PhC slabs the modes can be classified into TE-like (even) and TM-like (odd) modes based on their symmetry with respect to the z -plane which bisects the slab. Even modes have an even z -component of magnetic

field and odd modes an odd z -component of magnetic field and form two orthogonal bases. When a PhC slab is asymmetric, as is the case for the SOI slab, the modes can no longer be classified as purely even or odd modes. The modes can still be classified according their parities however, with respect to the z -plane. The parity of a state is defined as the expected value for a mirror operation with respect to the z -plane. For truly even and odd states the parity is +1 and -1 , respectively, while all other states have parity in between. Even-like states have parities larger than zero and odd-like states smaller than zero. Interaction between these modes of different parity is now allowed and can significantly contribute to additional propagation losses. This problem was mentioned in several reports^{1,9}, however the effect of asymmetry on transmission characteristics and propagation losses was not analyzed in detail.

A. Fitting of Transmission Spectra with a Photonic Band Structure

We can argue that the numerous narrow stop bands correspond to frequencies where the TE-like fundamental mode interacts with the TM-like slab modes at corresponding crossing points on the band diagram. In order to explain our experimental findings we performed extensive photonic band structure calculations to explore the parameter space to obtain the best fit for the spectral positions of the stop bands and cut-offs. Five structural parameters were explored for both TM and TE-like polarizations: slab thickness, hole diameter D , lattice constant a , width of the trench W_a and width of the central embedded strip W . Although these parameters can be measured from SEM images, the accuracy of these measurements typically lies within 3–5% and the photonic band structure is very sensitive to such small variations. For example a 5% change in the width of the embedded strip waveguide W (~ 13 nm) results in a 10% frequency shift of the stop band due to BZ folding of the fundamental TE-like mode. In addition to variations of the structural parameters the refractive indices of the buried oxide and of the silicon slab can easily differ by a similar amount from tabulated numbers due to different processing conditions. That finally defines a huge 7 parameter phase space to explore. At the same time the accuracy of the plane wave method strongly depends on the number of plane waves per lattice constant. In order to resolve for example a 5% difference in the width of the embedded waveguide W , the number of plane waves per lattice constant in this direction should be 16, which leads to an error in computed eigenfrequencies of around 1%. Increasing the number of plane waves to 32 results in a large increase of the required computer memory and simulation time. Fortunately the fitting of the dispersion of the TE-like mode and TM-like slab modes can be separated to some extent because the former is defined mainly by the thickness of the slab and the width of the strip

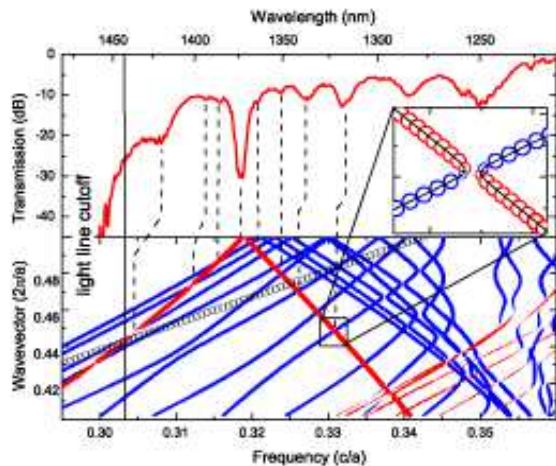


FIG. 5: Top panel: transmission spectrum for TE polarization of the double-trench PhC waveguide of 2 mm length normalized on transmission through a reference optical circuit. Bottom panel: projected photonic band structure of the asymmetric double-trench PhC waveguide. Blue (red) circles represent modes of positive (negative) parity. The size of the circles corresponds to the magnitude of the parity. Open circles correspond to the light line in oxide substrate. Inset: Enlarged portion of the photonic band structure

waveguide W , while the latter is defined predominantly by the diameter of the holes D and lattice constant a . This procedure is equivalent to simply overlapping the band diagrams of Figs. 1(a) and 1(b) and shifting one with respect to the other along the frequency axis.

The fitting strategy we employed consisted of fitting the cutoff and central zone-folding related dip in the TE spectrum by adjusting the width W of the strip waveguide, then changing the hole diameter D to find the frequencies of the anti-crossing, and finally comparing them with experimental data. To fine tune the fit the remaining structural parameters were scanned.

B. Positive and Negative Parity Mode Mixing in the Spectra for TE-polarized Input

Figure 5 shows the fitting of the transmission spectrum of the waveguide of 2 mm length for the TE polarization by photonic band structure calculations.

The narrow stop bands in the spectrum at frequencies 0.335, 0.331, 0.328, and 0.313 (wavelength of 1318, 1336, 1352 and 1414 nm, respectively) can be traced to the regions of crossing of the negative parity (TM-like) slab-confined modes and fundamental positive parity (TE-like) mode. The inset in Fig. 5 is a blown-up image of the phase space around one such region at a frequency of $0.331c/a$. It can be clearly seen that the interaction between the modes results in the anti-crossing

behavior with gradual change of the parity from negative to positive values for the states at the stop band edges. This represents mode mixing of the TE-like and TM-like modes. The width of the stop band can be measured as $3.4 \times 10^{-4}(c/a)$, which is roughly 2.5 times wider than experimentally measured and is probably not completely resolved by finite mesh resolution in the calculations. The states at the stop band edges are mixed states that correspond to conversion of the fundamental predominantly TE-like mode into predominantly TM-like slab modes. The latter being less confined in the center of the waveguide could not be coupled efficiently to the output access strip waveguide. This effect is the origin of observed dips in the transmission spectra. Further analysis of the Fig. 5 based on the same interpretation allows weak resonances at frequencies 0.319, 0.321, and 0.325 (wavelength of 1394, 1386 and 1352 nm) also to be assigned to anti-crossing regions.

For short waveguides the dips appear to be much broader than for the 2mm long device. Such behavior can be explained by the finite-size effect that is well documented for photonic crystals. This length-dependent broadening results in the possibility of conversion of predominantly TE-like fundamental mode into TM-like modes even at frequencies far away from the stop bands. This effect can be responsible for relatively high losses encountered by the TE-like mode measured from Fig. 3 and is expected to apply to any asymmetric SOI photonic crystal waveguides.

C. Mode Mixing in the Spectra for TM-polarized Input

Figure 6 compares the experimental transmission spectrum for a 2-mm-long double-trench PhC waveguide with a TM polarized input with the band diagram obtained using the structural parameters resulting from the fitting as used in Fig. 5.

The stop band at 1328 nm can be assigned to the zone-folding of the fundamental mode at the BZ edge at frequency of $0.330c/a$. Narrow stop bands visible at frequencies of 0.325, 0.335 and $0.342c/a$ (wavelength of 1344, 1307 and 1284 nm) can be readily assigned to stop bands due to interaction of the fundamental mode with the slab modes in direct analogy to the interpretation of the TE polarized spectra. Indeed for each of these frequencies the small gap can be found in the fundamental mode dispersion curve, which occurs due to anti-crossing with the corresponding slab mode. This is illustrated in the inset of Fig. 6, where a magnified portion of the band diagram is shown in the vicinity of the stop band around $0.342c/a$.

VI. CONCLUSION

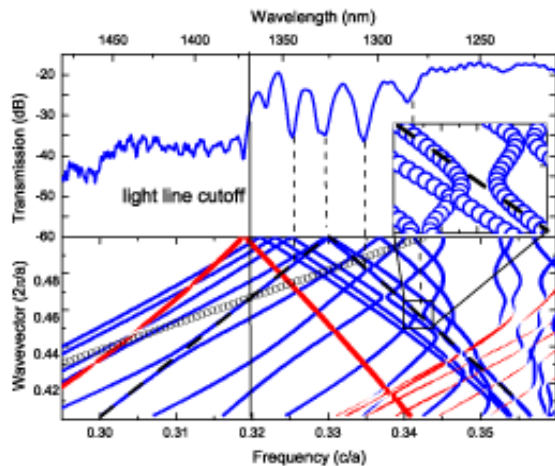


FIG. 6: Top panel: transmission spectrum for TM polarization of the double-trench PhC waveguide of 2 mm length normalized on transmission through a reference optical circuit. Bottom panel: projected photonic band structure of the asymmetric double-trench PhC waveguide. Blue (red) circles represent modes of positive (negative) parity. The size of the circles corresponds to the magnitude of the parity. Open black circles correspond to the light line of the oxide substrate. Inset: Enlarged portion of the photonic band structure.

The novel design of the double-trench PhC waveguide with a single-mode strip waveguide core is analyzed, fabricated and optically characterized. The waveguiding of the TE-polarized light is characterized by a large bandwidth with relatively low-loss transmission (50 dB/cm). However inherent asymmetry of the SOI-based double-trench PhC structures induce weak coupling of the modes of different polarizations, which result in the appearance of multiple narrow stop bands and additional attenuation. Detailed interpretation of the spectral features found in experimental transmission spectra is possible for the first time owing to data that compares closely to the spectra obtained from photonic band structure calculations. While this analysis was performed on the double-trench PhC waveguide, the effects of cladding asymmetry are equally relevant to other types of PhC waveguides.

Acknowledgments

The authors are grateful to Prof. Shanhui Fan (Stanford University) for sending us his manuscript prior to publication and fruitful discussions. The authors also gratefully acknowledge the contributions of the MRL staff at the IBM T. J. Watson Research Center and in particular Ed Sikorski for his etch expertise.

* Corresponding author; e-mail: yvlasov@us.ibm.com

¹ S. G. Johnson, P. R. Villeneuve, S. Fan, and J. D. Joannopoulos, *Phys. Rev. B* **62**, 8212, 2000.

² A. Chutinan and S. Noda, *Phys. Rev. B* **62**, 4488, 2000.

³ M. Loncar, D. Nedeljkovic, T. Doll, J. Vuckovic, and A. Scherer, *Appl. Phys. Lett.* **77**, 1937, 2000.

⁴ M. Notomi, K. Yamada, A. Shinya, J. Takahashi, C. Takahashi, and I. Yokohama, *Phys. Rev. Lett.* **87**, 253902, 2001.

⁵ S. J. McNab, N. Moll, and Yu. A. Vlasov, *Optics Express*, **11**, 2927, 2003.

⁶ W. T. Lau, and S. Fan, *Appl. Phys. Lett.* **81**, 3915, 2002.

⁷ T. Søndergaard and A. Lavrinenko, *Optics Commun.* **203**, 263, 2002.

⁸ S. McNab, N. Moll, and Y. Vlasov, preprint, 2003.

⁹ Min Qiu, *Phys. Rev. B* **66**, 033103, 2002.

¹⁰ S. G. Johnson and J. D. Joannopoulos, *Optics Express* **8**, 173, 2001.

¹¹ H. Kogelnick and C.V. Shank, *J. Appl. Phys.* **43**, 2328 (1972).